Crack-Tip Equation of Motion Due to Nonuniform Residual Stresses in a Weldment

The dynamic stress intensity and dynamic fracture toughness as functions of the crack speed are used in the derivation of the crack-tip equation of motion.

BY C.-K. FANG, E. KANNATEY-ASIBU, JR., AND J. R. BARBER

ABSTRACT. On the basis of the fracture criterion, a crack-tip equation of motion has been derived for a rectangular through crack due to nonuniformly distributed residual stresses in a weldment. The dependence of the dynamic stress intensity factor and dynamic fracture toughness on crack speed was employed in the derivation. The effect of crack-tip bluntness and the difference between initiation toughness and arrest toughness were also considered. This model gives better correlation with experimental data on limiting crack speed obtained from the literature, as compared with other models. Variations in crack length and crack speed with time have also been obtained. The effects of bluntness parameters and initial crack length on crack growth behaviors have been investigated in detail.

Introduction

The study of crack speed is essential in the field of dynamic fracture mechanics, especially when analyzing the dynamic response due to a rapidly propagating crack using acoustic emission. Particularly in the case of a weldment, where the residual stress developed during cooling is nonuniformly distributed, the crack-speed function as the crack propagates can be quite complicated.

The longitudinal residual stress in a weldment is usually highest along the weld centerline, diminishes in the transverse direction, and is balanced by compressive stresses in the rest of the weldment. In the tension zone of the weldment, some defects or initial cracks may exist due to hot cracking during solidification. Crack propagation can be initiated from such defects or initial cracks.

Crack motion in brittle materials subjected to uniform loading has been extensively studied. Extending Griffith's theory by including the kinetic energy effect, Mott (Ref. 1) gave the first quantitative prediction for the speed of a central crack propagating rapidly under a uniform remote stress in an infinite body. His derivation assumed that the crack speed v is independent of the crack length a, *i.e.*, $dv/da = 0$. He argued that the velocity of crack propagation, under uniform stress, of a crack in a material that is not ductile, will tend toward a value of the order of the velocity of sound in the material, which is independent of the velocity of the applied stress or the atomic cohesive forces across the cleavage plane.

Mott's result was refined by Berry (Ref. 2) and Dulaney and Brace (Ref. 3) by removing the assumption that $dv/da = 0$. They obtained the limiting crack speed as $0.38C_0$, where C_0 is the velocity of elastic waves undergoing one-dimensional wave propagation in a thin rod. Kanninen and Popelar (Ref. 4) incorporated the kinetic energy into the dynamic energy release rate, which is a combination of kinetic energy and potential energy change. They re-derived the crack-tip motion by applying Freund's dynamic approach (Refs. 5, 6). Although their derivation is more rigorous, the experimental data for limiting crack speeds, $0.2C_0$ to $0.42C_0$ for most metals and glasses (Ref. 7), are closer to the earlier result, $0.38C_0$ (Ref. 3). (The elimination of such a discrepancy is one of the objectives of our present work.) Bergkvist (Ref. 8) considered a crack-speed-dependent fracture toughness in his derivation of crack motion. By equating the dynamic energy release rate to the fracture energy, he derived the crack-tip equation of motion and gave a numerical result for a brittle central crack subjected to a uniform extension load. The initial crack motion of a Griffith crack was derived by Rose (Ref. 9). By introducing a slight perturbation, which makes the stress intensity factor larger than the fracture toughness, he obtained an approximation to the equation of motion for the unstable growth of a Griffith crack. By considering a slightly blunted crack, Freund (Ref. 10) derived the equation of motion for a half plane crack subjected to an opposite pair of concentrated forces in an otherwise unbounded elastic solid. Again, his result was under the assumption of constant fracture energy, although the dynamic energy release rate was considered as a function of crack speed. Recently, Xu and Needleman (Ref. 11) developed the cohesive zone model for dynamic fracture, where the cohesive surface constitutive relation was obtained. Of these authors, only Bergkvist (Ref. 8) considered the dependence of dynamic fracture toughness on crack speed, and his derivation was based upon the assumption that the initial crack half length $a_0 \approx 0$ or a_0 is much less than the instantaneous crack half length a.

KEY WORDS

Crack Propagation
Residual Stress
Weldment
Dynamic Stress Intensity Factor
Dynamic Fracture Toughness
Bluntness
Limiting Crack Speed

C.-K. FANG is an Associate Professor with the Department of Mechanical Engineering, China Institute of Technology and Commerce, Nankang, Taipei, Taiwan, R.O.C. E. KANNATEY-ASIBU, JR., and J. R. BARBER are Professors with the Department of Mechanical Engineering and Applied Mechanics, University of Michigan, Ann Arbor, Mich.

In this article, we use the dynamic stress intensity and dynamic fracture toughness as functions of crack speed in the derivation of the crack-tip equation of motion and consider the effect of bluntness of the crack tip, as well as the difference between the initiation and arrest fracture toughness. The method is applied to the case of crack propagation in a weldment with a nonuniform distribution of residual stress. The crack growth model in this article is compared with other models in the literature and experimental results, all of which relate to the case of uniform remote stress — a special case in our model. Finally, the numerical results of crack growth will provide the data necessary for determining the crack opening displacement, and thereby afford opportunities for obtaining the dynamic response at a field point due to a cracking source.

Background

Dynamic Stress Intensity Factor

Consider a semi-infinite crack on the plane $\xi_2 = 0$ in an otherwise unbounded body subjected to general time-independent loading. The crack tip is stationary until the instant of crack growth onset. It then propagates in the ξ_1-direction with instantaneous crack-tip location $\xi_1 = a$ and crack speed v (= da/dt). The propagation of the crack depends only on the local asymptotic stress field near the crack tip. For small scale yielding, propagation of a crack in mode I fracture is governed by the instantaneous stress intensity factor $K_I(a,v)$ — often termed the dynamic stress intensity factor for opening mode. It has the following form (Refs. 5, 6, 10, and 12):

$$K_I(a,v) = k(v)\, K_I(a,0), \qquad (1)$$

where $K_I(a,0)$ is the equilibrium stress intensity factor for the specified time-independent loading, $k(v)$ is a universal function of instantaneous crack speed given by (Ref. 10)

$$k(v) = \frac{1 - v/C_R}{\sqrt{1 - v/C_d}}, \qquad (2)$$

C_d is the dilatational (or longitudinal) wave speed and C_R is the Rayleigh wave speed. Thus

$$K_I(a,v) = \frac{1 - v/C_R}{\sqrt{1 - v/C_d}}\, K_I(a,0), \qquad (3)$$

which has been proven to be valid for arbitrarily varying crack speeds (Ref. 12). The relationship between $k(v)$ and crack speed is also depicted in Fig. 1.

Note that the above equation is only valid for mode I loading. If the crack is curved, mixed-mode loading occurs, and $k(v)$ will take a different form for different fracture modes (Ref. 12). We will not consider crack curving in this research. We note that Equation 3 was developed for an infinite body. It is also valid, however, for a finite body, so long as the reflected stress waves from the nearest boundary have not yet impinged upon the crack tip (Ref. 4). Furthermore, the assumption of a semi-infinite crack means that the loading due to the stress waves generated by the propagation of the other crack tip, if one exists, was not considered in Equation 3. This assumption, however, can be eliminated if the stress wave generated at the other tip of a finite crack has not yet reached the crack tip of interest, or if it is negligible in amplitude. For engineering consideration, its amplitude is negligibly small compared to the magnitude of critical stress for crack extension.

Dynamic Fracture Toughness

During crack propagation, the dynamic stress intensity factor K_I must always be equal to the dynamic fracture toughness K_{ID} of the material, *i.e.*,

$$K_I(a,v) = K_{ID}. \qquad (4)$$

The dynamic fracture toughness K_{ID} can be determined experimentally by using optical methods combined with high-speed photography. The photoelastic and caustic (shadow spot) methods are widely used. The dynamic stress intensity factor can be calculated by observing the fringe pattern and the shadow spot, respectively, at the crack tip from high-speed photography, where the instantaneous value that the stress intensity factor assumes is the dynamic fracture toughness K_{ID}. The relationship between dynamic fracture toughness K_{ID} and crack speed[1] has been obtained by a number of researchers (Refs. 13–16). All these authors obtained results of the general form shown in Fig. 2. In general, the crack speed is observed to have relatively little influence on the dynamic fracture toughness at low crack speeds, but K_{ID} increases rapidly as the crack speed approaches a certain limiting speed v_c, sometimes called the terminal velocity. As mentioned by Kanninen

1. *This involves the tacit assumption that the dynamic fracture toughness depends on the crack speed only (and in particular is independent of acceleration). This assumption is valid for comparatively brittle materials (Ref. 8).*

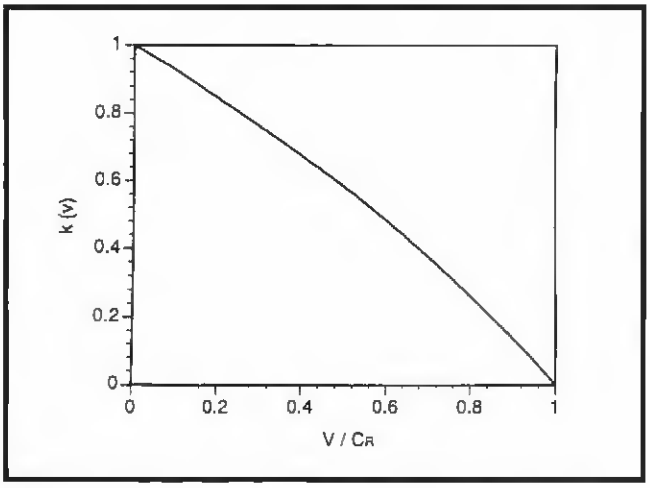

Fig. 1 — Relationship between k(v) and normalized crack speed.

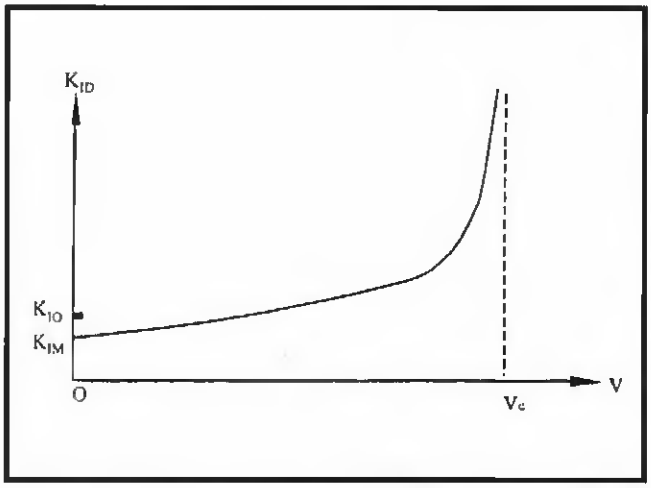

Fig. 2 — Relationship between dynamic fracture toughness and crack speed.

and Popelar (Ref. 4), the limiting speed depends neither on the manner of producing the crack nor upon the applied stress, and it ranges from $0.2C_o$ to $0.4C_o$ (Ref. 7) for most glasses and metals. In Fig. 2, K_{IO} is the initiation fracture toughness for an initially sharp crack tip, and K_{IM} is the fracture toughness corresponding to zero crack speed and therefore also describes the condition at the instant of crack arrest.

The K_{ID}–v curve can be approximated by the following empirical equation (Ref. 4):

$$K_{ID} = \frac{K_{IM}}{1-\left[\frac{v}{v_c}\right]^n}, \qquad (5)$$

where $n > 0$ is a dynamic shape factor, and K_{IM}, v_c, and n are to he determined experimentally.

General Crack-Tip Equation of Motion

The governing equation for crack-tip motion can now be obtained by substituting Equations 3 and 5 into Equation 4, resulting in the following ordinary differential equation:

$$\frac{1-\frac{1}{C_R}\frac{da}{dt}}{\sqrt{1-\frac{1}{C_d}\frac{da}{dt}}}\,K_I(a,0)=\frac{K_{IM}}{1-\left[\frac{1}{v_c}\frac{da}{dt}\right]^n}, \qquad (6)$$

for a, where v has been replaced by da/dt. Solving this equation, we can obtain the crack-tip speed. Crack arrest will occur when $K_I(a,v) \le K_{IM}$.

Propagation under a Nonuniform Stress

Consider a rectangular through crack in the plane $\xi_2 = 0$ with crack tips initially at $\pm a_o$ at the weld joint in a large thin plate — Fig. 3. The longitudinal residual stress that develops in the ξ_2-direction during cooling may cause brittle crack propagation in the ξ_1-direction in a high-hardenability material. We make the following assumptions: 1) that the material is homogeneous and isotropic and that the plate has cooled to the temperature range in which the material behavior is linearly elastic; 2) that the crack propagates in an infinite plate, which is appropriate as long as the plate is large enough for the fracture process to be completed before the reflected stress waves generated from the fracture impinge on the crack; 3) that the crack propagates symmetrically with respect to the plane $\xi_1 = 0$ at variable crack speeds with instantaneous crack-tip locations at $\xi_1 = \pm a$.

According to Josefson's (Ref. 17) study of the welding residual stress in a thin plate (4.6 mm thick), the through-thickness stress variation is small. As a result, we can assume that the stress field is uniform in the ξ_3-direction for the thin plate. The distribution of longitudinal residual stress σ_R in the weld joint is found experimentally to have the form illustrated in Fig. 4 (Refs. 18–20). This curve can be approximated by the equation (Ref. 21)

$$\sigma_R(\xi_1) = \sigma_o\left\{1-\left[\frac{\xi_1}{c}\right]^2\right\}\exp\left\{-\frac{1}{2}\left[\frac{\xi_1}{c}\right]^2\right\}, \qquad (7)$$

where c is the half-width of the tension zone and σ_o is the maximum tensile residual stress at the weld center. The value of σ_o is less than or approximates the yield strength σ_Y of the material, and the value of $\sigma_Y - \sigma_o$ increases with an increase in yield strength (Ref. 21).

Note that the stress distribution given in Equation 7 is only valid for a weldment without cracks. Once a crack forms, the stress is redistributed. We assume that the crack is far from both ends of the weld, so that the residual stress redistribution can be ignored and Equation 7 is still valid during crack propagation. The equilibrium stress intensity factor $K_I(a,0)$ is the same as that of a crack opened by normal tractions equal and opposite to $\sigma_R(\xi_1)$ in an otherwise stress-free body (Ref. 22). Now $K_I(a,0)$ can be obtained by the superposition of the general solution for a pair of eccentric point forces of magnitude P acting on the upper and lower crack faces — Fig. 5. The equilibrium stress intensity factor for the right crack tip for such a concentrated loading condition is (Refs. 23, 24)

$$K_I(a,0)=\frac{P}{\sqrt{\pi a}}\sqrt{\frac{a+\xi_1}{a-\xi_1}}. \qquad (8)$$

By superposition, the equilibrium stress intensity factor for a crack subjected to the nonuniform pressure of magnitude $\sigma_R(\xi_1)$ is given by the integral

$$K_I(a,0)=\frac{1}{\sqrt{\pi a}}\int_{-a}^{a}\sigma_R(\xi_1)\sqrt{\frac{a+\xi_1}{a-\xi_1}}\,d\xi_1. \qquad (9)$$

Employing the residual stress distribution $\sigma_R(\xi_1)$ given by Equation 7, this integral becomes

$$K_I(a,0) = 2\sigma_o f(a/c)\sqrt{\frac{a}{\pi}}, \qquad (10)$$

where

$$f(a/c)=\int_0^{a/c}\left[1-\zeta^2\right]\exp\left[-\frac{\zeta^2}{2}\right]\times\sqrt{\frac{1}{(a/c)^2-\zeta^2}}\,d\zeta, \qquad (11)$$

and $\zeta = \xi_1/c$. Note that $K_I(a,0) \to \sigma_o(\sqrt{\pi a})^{1/2}$ if $c \to \infty$, which converges to

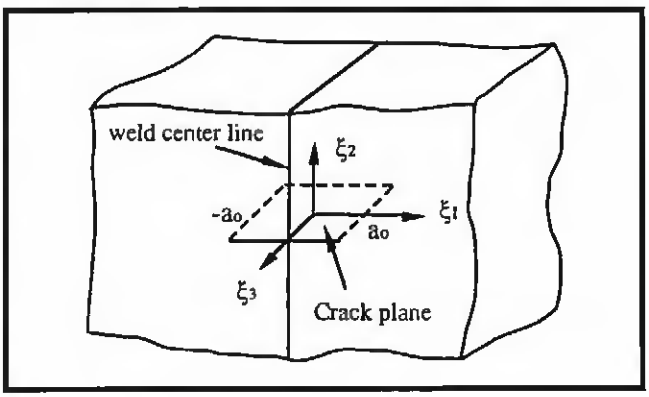

Fig. 3 — A rectangular crack in a weldment.

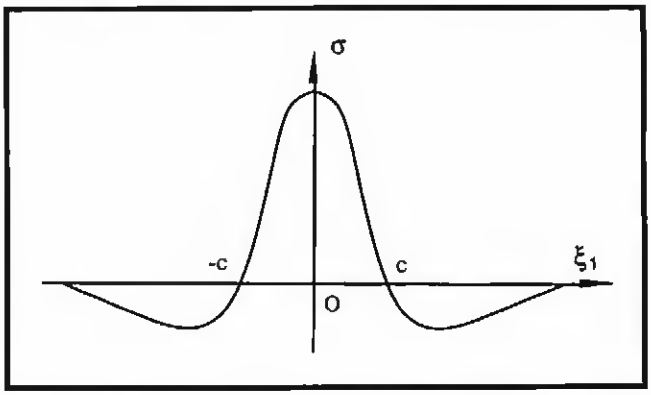

Fig. 4 — Longitudinal residual stress distribution in a weldment.

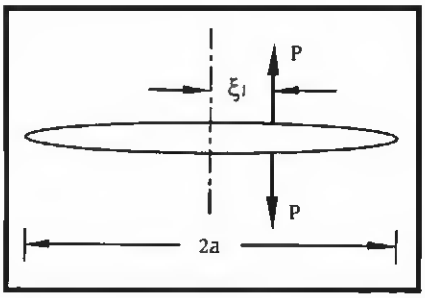

Fig. 5 — Crack with a pair of eccentric concentrated forces.

the equilibrium stress intensity factor of a central through crack under uniform remote stress σ_o. The function f(a/c) has a zero at the critical value a* = 1.78c and is positive in 0 < a < a* and negative in a > a*. It follows that a crack cannot propagate beyond a = a*.

As the weldment cools, the residual stress increases gradually, as do the stress intensity factor and energy release rate for virtual crack growth. Eventually the crack may start to propagate if σ_o is high enough. At the moment just before crack growth, we have $a = a_o$ and v = 0, and the crack will start to propagate when the equilibrium stress intensity factor $K_I(a_o,0)$ is equal to the fracture toughness, K_{IO}.

Note that if the initial crack is not perfectly sharp, a somewhat higher value of $K_I(a_o,0)$ is needed to initiate crack propagation, and this effect is described by defining an apparent fracture toughness:

$$K_{IO}' \sqrt{n_b}\, K_{IO}, \tag{12}$$

where n_b is known as the bluntness parameter. The value of n_b is related to the root radius of the initial crack tip (Ref. 25). The relation between K_{IO}' and notch root radius can be obtained from Ref. 26 for alloy steels and Ref. 27 for AISI 4340 steel. With this notation, the condition for the initiation of crack propagation is

$$K_I(a_o,0) = \sqrt{n_b}\, K_{IO}. \tag{13}$$

Substituting Equation 10 into Equation 13, we have

$$2\sigma_o f(a_o/c)\sqrt{\frac{a_o}{\pi}} = \sqrt{n_b} K_{IO} \tag{14}$$

from which we obtain the critical σ_o for crack initiation as

$$\sigma_o = \frac{K_{IO}\sqrt{\pi n_b/a_o}}{2f(a_o/c)}. \tag{15}$$

Once the crack starts to extend, crack propagation is governed by Equation 6, where

$$K_I(a,0) = K_{IO}\frac{f(a/c)}{f(a_o/c)}\sqrt{\frac{n_b a}{a_o}}, \tag{16}$$

from Equations 10 and 15. Substituting Equation 16 into Equation 6, we obtain a differential equation:

$$\frac{1-\frac{1}{C_R}\frac{da}{dt}}{\sqrt{1-\frac{1}{C_d}\frac{da}{dt}}}\left\{1-\left[\frac{1}{v_c}\frac{da}{dt}\right]^n\right\} = \left[\frac{K_{IM}}{K_{IO}}\right]\frac{f(a_o/c)}{f(a/c)}\sqrt{\frac{a_o}{n_b a}} \tag{17}$$

for the instantaneous crack half-length, a.

The initial crack speed immediately after the onset of crack growth, v_o, can be obtained by substituting $a = a_o$ in Equation 17, giving

$$\frac{1-v_o/C_R}{\sqrt{1-v_o/C_d}}\left\{1-\left[\frac{v_o}{v_c}\right]^n\right\} = \frac{K_{IM}}{K_{IO}}\sqrt{\frac{1}{n_b}}. \tag{18}$$

It is evident that v_o depends on the bluntness parameter n_b but is independent of the initial crack length a_o and the half-width c of the tension zone. This is to be anticipated because the initial crack speed can only depend on the local conditions at the crack tip immediately before propagation starts, and these are characterized completely by bluntness and fracture toughness. Thus Equation 18 also applies to more general fracture geometries and loading conditions. If the right-hand side of Equation 18 is unity — *i.e.*, if the crack is sharp ($n_b = 1$) and $K_{IO} = K_{IM}$ — then this equation has the trivial solution $v_o = 0$, because $C_d > C_R$ and n > 0. For $K_{IM}/(K_{IO}\sqrt{n_b})$ slightly less than unity, $v_o << \{v_c, C_R, C_d\}$, and an approximate solution to Equation 18 can be obtained by expanding the left side and dropping higher order terms, with the result

$$v_o = \frac{1-\frac{K_{IM}}{K_{IO}}\sqrt{\frac{1}{n_b}}}{\frac{1}{C_R}-\frac{1}{2C_d}}. \tag{19}$$

The final crack half-length a_f is obtained by substituting da/dt = 0 in Equation 17, giving

$$\frac{f(a_o/c)}{f(a_f/c)}\sqrt{\frac{a_o}{n_b a_f}} = \frac{K_{IO}}{K_{IM}}. \tag{20}$$

Numerical Procedure

Equations 17 and 18 cannot be solved explicitly and require a numerical solution. Given the initial crack half-length, a_o, the bluntness parameter, n_b, the parameters of the empirical $K_{ID} - v$ curve, and the stress wave speeds for the material, the initial crack speed v_o can be calculated iteratively by Newton's method from Equation 18. Once the initial crack speed is obtained, the crack half length after a small time increment δt can be calculated, and the new crack speed da/dt can be obtained by iterative solution of Equation 17. This procedure is repeated for subsequent time increments until the crack speed falls to zero, when crack arrest will occur. Once a and da/dt are known as functions of time, the dynamic stress intensity factor $K_I(a,v)$ can be calculated from Equations 3 and 16.

Adequate convergence of the algorithm was obtained using a time increment of 0.25 μs, which was therefore used throughout the following work.

Results and Discussion

To illustrate the use of the method, we consider the dynamic fracture of AISI 4340 steel, for which the wave speeds are C_d = 6201 m/s and C_R = 3217 m/s (Ref. 28).

Dynamic fracture toughness measurements for this material have been performed by Dally (Ref. 13), Rosakis, *et al.* (Ref. 14), and Zehnder, *et al.* (Ref. 16). The results, summarized in Table 1, show that K_{IM} falls in the range 52–62 MPa $m^{1/2}$ for specimens with hardnesses in the range 45–50 Rockwell C. Values of v_c and n were obtained by fitting a curve of the form of Equation 5 to the experimental data of Dally (Ref. 13) and Rosakis (Ref. 14). In both cases, a good fit was obtained with v_c = 1250 m/s and n = 1.75. These values are used in the following simulation, with K_{IM} = 52 MPa $m^{1/2}$ and K_{IO} = 61 MPa $m^{1/2}$ from Dally (Ref. 13).

Table 1 — Arrest Fracture Toughness for 4340 Steel with Different Hardness

	K_{IM} (MPa $m^{1/2}$)	Hardness (HRC)
Dally [1979]	52	46
Rosakis, *et al.* [1984]	≈56	45
Zehnder, *et al.* [1990]	62	50

Crack Propagation Under Uniform Remote Stresses

We first consider the simple case of a central through crack in a plate subjected to a uniformly distributed remote stress. This can be considered as the limiting case in which $c \to \infty$ (see Equation 7), for which Equation 17 reduces to

$$\frac{1-\frac{1}{C_R}\frac{da}{dt}}{\sqrt{1-\frac{1}{C_d}\frac{da}{dt}}}\left\{1-\left[\frac{1}{v_c}\frac{da}{dt}\right]^n\right\} = \left[\frac{K_{IM}}{K_{IO}}\right]\sqrt{\frac{a_o}{n_b a}}. \qquad (21)$$

Figure 6A shows the relationship between the normalized crack speed v/C_R and normalized crack length a/a_o. The difference between the fracture toughness for initiation K_{IO} and for arrest K_{IM} has been neglected in Curve 1, while K_{IM}/K_{IO} is taken as 52/61 in Curve 2. As can be seen in both curves, the crack speeds rise rapidly in the beginning, and then level off without exceeding the limiting crack speed v_c = 1250 m/s = $0.388C_R$. The detailed behavior in the initial stages of crack propagation, Fig. 6B, shows that the crack growth starts from zero crack speed in Curve 1, while there is a jump in crack speed of magnitude about $0.1C_R$ in Curve 2 due to the departure of K_{IM} from K_{IO} as predicted by Equation 19.

The propagation speeds for cracks with different bluntness parameters are depicted in Fig. 7A, where K_{IM}/K_{IO} is again taken as 52/61. The detailed initial behavior is illustrated in Fig. 7B. Curve 1 represents the behavior of a sharp crack starter, while Curves 2 and 3 are for bluntness parameters 1.5 and 2, respectively. The jump in crack speed as predicted by Equation 19 is evident in each case. The shape of these curves and the characteristic of speed jump are similar to the experimental curves shown by Dulaney and Brace (Ref. 3), where the material used was polymethyl methacrylate with a sawed slit in a large specimen of dimensions 200 x 63 x 0.64 cm. Equation 19 shows that the speed jump is due to both bluntness and the departure of K_{IM} from K_{IO}. Thus it occurs even for a sharp crack starter (n_b = 1) as shown in Curve 1. The speed jump increases with an increase of bluntness parameter due to the higher strain energy stored before the onset of crack growth. The magnitudes of these jumps are $0.16C_R$ for n_b = 1.5 and $0.19C_R$ for n_b = 2.

Crack Propagation under Nonuniform Residual Stresses

We now consider the case of cracking due to the nonuniform residual stress of Equation 7. Figures 8–14 show numerical results obtained from the above procedure, the half-width, c, of the tension zone being 22.5 mm, and K_{IO}/K_{IO} = 52/61.

Figures 8–10 show the crack propagation behavior for four cracks of the same initial half-length, 2.5 mm, but of different bluntness parameters. In each figure, Curve 1 represents the results for an initially sharp crack with bluntness n_b = 1, while those for blunt crack tips are shown

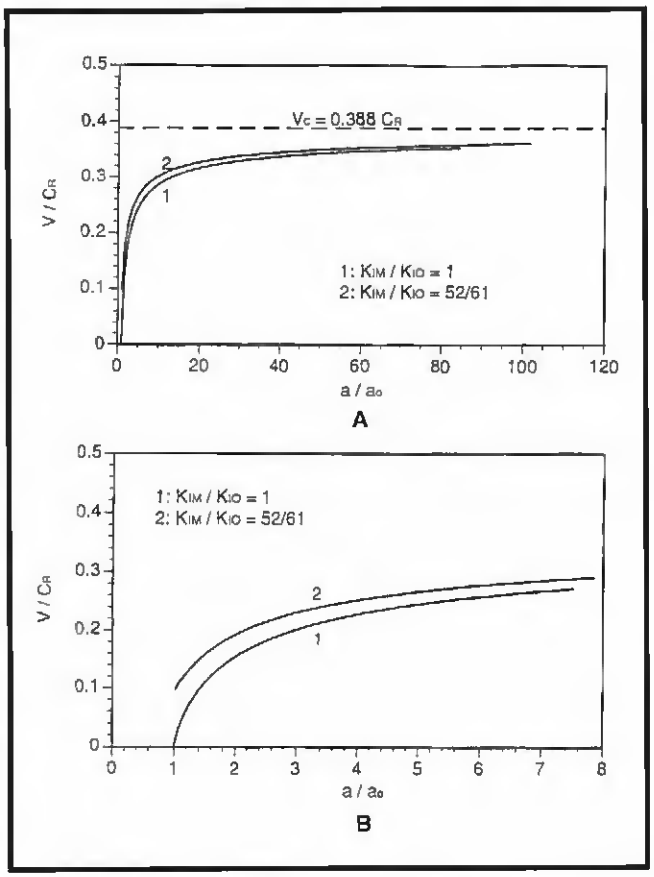

Fig. 6 — Relationship between normalized crack speed and normalized crack length for a 4340 steel plate containing an initially sharp (n_b = 1) central through crack subjected to a uniformly distributed remote stress. A — Overview; B — detailed behavior in the initial stages.

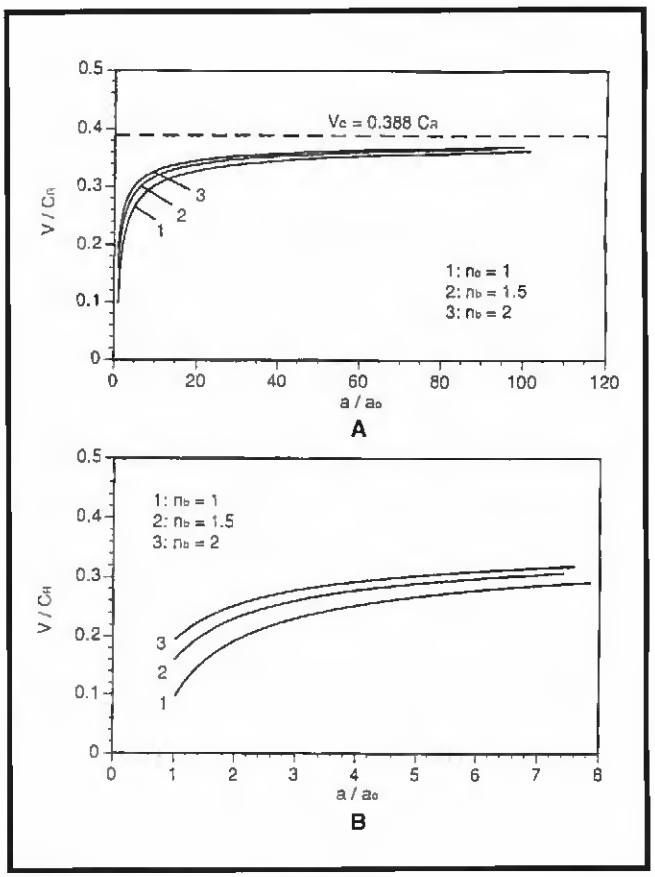

Fig. 7 — Relationship between normalized crack speed and normalized crack length for a 4340 steel plate containing a central through crack with different initial bluntness parameters subjected to a uniformly distributed remote stress (K_{IM}/K_{IO} = 52 / 61). A — Overview; B — detailed behavior in the initial stages.

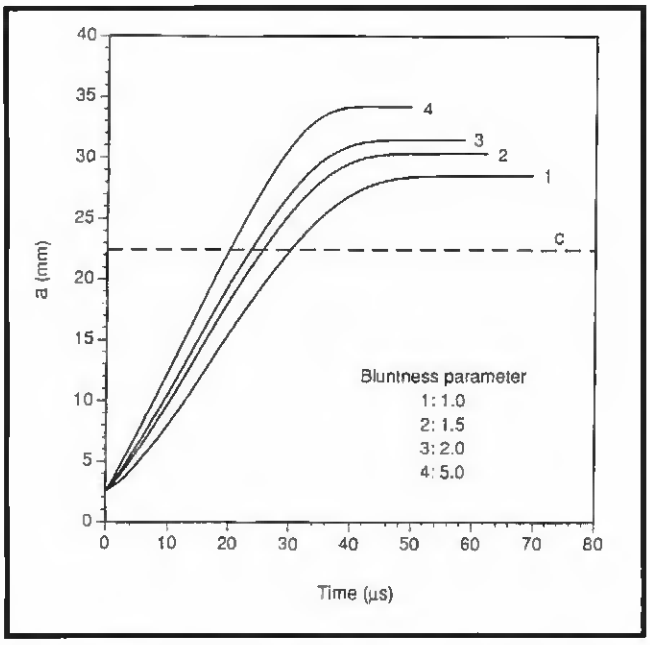

Fig. 8 — Instantaneous crack length as a function of time for cracks, with the same initial crack length but different bluntness parameters, subjected to a nonuniformly distributed residual stress in a 4340 steel plate (dashed line shows c = 22.5 mm).

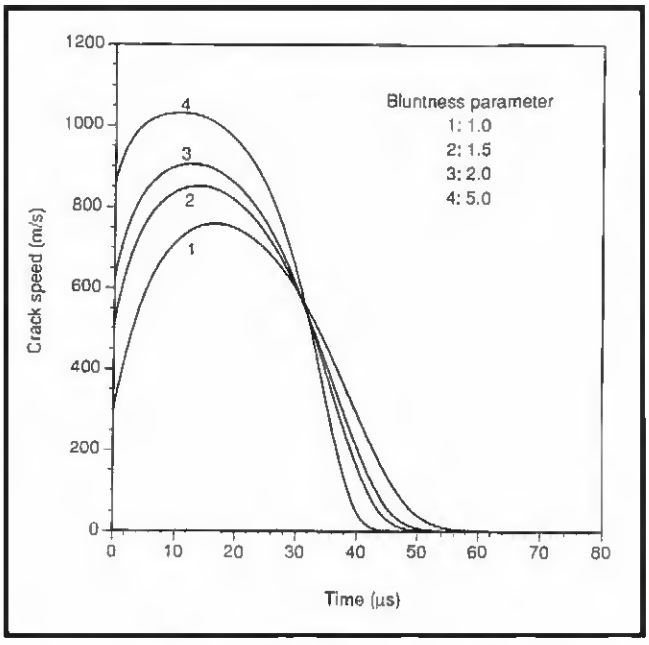

Fig. 9 — Crack speed behavior as a function of time for cracks, with the same initial crack length but different bluntness parameters, subjected to a nonuniformly distributed residual stress in a 4340 steel plate (c = 22.5 mm).

in Curves 2 (n_b = 1.5), 3 (n_b = 2), and 4 (n_b = 5).

As can be seen in Fig. 8, the crack length increases with time and then stops at a certain final length, with a_f = 28.6, 30.4, 31.5, and 34.3 mm for n_b = 1, 1.5, 2, and 5, respectively. A blunter crack stops sooner than a sharper one, but its final crack length is longer. Thus, although a blunt crack is safer than a sharp one from the point view of critical stress for crack initiation, it will propagate farther once the critical stress is reached. It also follows that an initially blunt crack propagates faster than a sharp one, as is also evident from the slopes of the curves in Fig. 8. The duration of crack propagation is shorter for a blunt crack.

Figure 9 shows the crack speed as a function of time for cracks with different bluntness parameters. The jump in crack speed at the onset of crack growth is evident in each curve. They are 301 m/s (n_b = 1), 509 m/s (n_b = 1.5), 619 m/s (n_b = 2), and 858 m/s (n_b = 5). After this jump, the crack speed increases until it reaches peak. It is then followed by a deceleration due to the decreasing residual stress farther from the weld centerline. As expected, the maximum crack speed is higher for a blunter crack because of the higher stress intensity factor required to initiate the crack propagation, resulting in higher strain energy stored in the specimen prior to crack growth. From these curves, it can be concluded that the variation of crack speed during propagation is smoother for a sharper crack, while a blunter one starts with a substantial jump in crack speed and is arrested in a more abrupt manner.

Figure 10 shows the corresponding dynamic stress intensity factor K_I as a function of time. The stress intensity factors required for crack initiation, which are equal to K_{IO}', are different for cracks with different bluntness parameters (see Equation 12). Once the crack starts growing, the stress intensity factor drops from the value of K_{IO}' at time $t = 0^-$ to a lower value at $t = 0^+$. This follows from Equation 3, which shows that $K_I(a_o,v) < K_I(a_o,0)$ and hence that the stress intensity factor must fall if $v_o \neq 0$ — *i.e.*, if with a nonzero initial speed. Afterward, the dynamic stress intensity factor increases due to the increase of crack length, followed by a decrease due to the diminution of the welding residual stress with position away from the weld centerline. Thus, there exists a peak in each curve. Eventually, the crack is arrested as K_I reaches the arrest fracture toughness K_{IM} as indicated by the lowest dashed line in Fig. 10. Like crack speed behavior, the variation of dynamic stress intensity factor is smoother for a sharper crack.

Figures 11–14 demonstrate the effects of initial crack length on crack growth behavior. Equation 15 shows that shorter cracks require a larger value of residual stress σ_o for initiation. However, once crack propagation starts, it progresses farther for initially short cracks than for long ones (Fig. 11), which shows the evolution of the crack length in time for initially sharp cracks of various lengths. In Fig. 12, the final crack half-length a_f is shown as a function of the initial half length a_o. In this figure we also include results for an initially blunt crack with n_b = 2. The value of a_f can never exceed 40 mm, beyond which f(a/c) < 0 and thus $K_I(a,v)$ < 0 from Equations 10, 11 and 3. It is also evident in Curves 1–3 of Fig. 11 that the duration of crack propagation is longer for a crack with a longer initial length. However, this trend becomes reversed if the initial crack length is very long (Curves 4–6). As a result, the largest duration of crack propagation occurs in Curve 4.

From Fig. 13, it is evident that both average and peak crack speeds are higher for a crack with a shorter initial length. In this aspect, a shorter initial crack has an effect similar to a blunter one on crack-speed behavior. However, in contrast to Fig. 9, the initial crack speeds are identical for cracks with different initial sizes. This is consistent with the conclusion from Equation 18 that the initial crack speed depends on the bluntness parameter but is independent of initial crack length. In addition, it is observed that

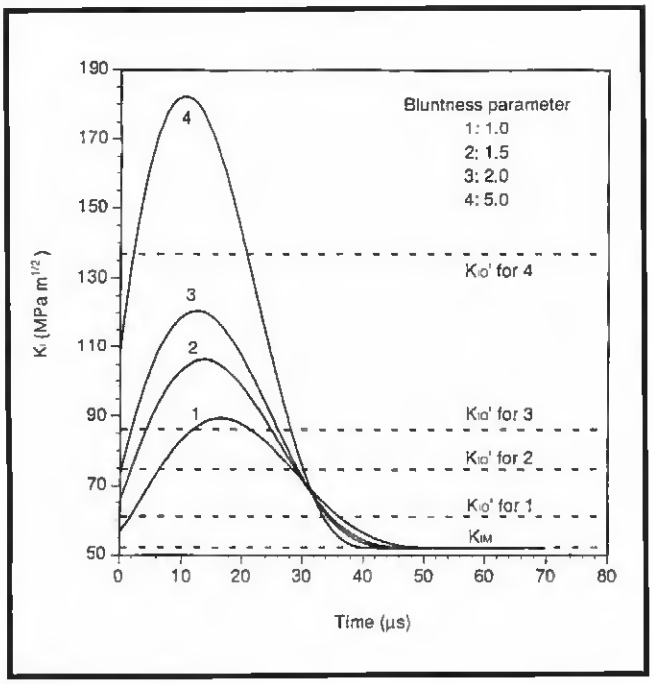

Fig. 10 — The variation of dynamic stress intensity factor as a function of time for cracks, with the same initial crack length but different bluntness parameters, subjected to a nonuniformly distributed residual stress in a 4340 steel plate (c = 22.5 mm).

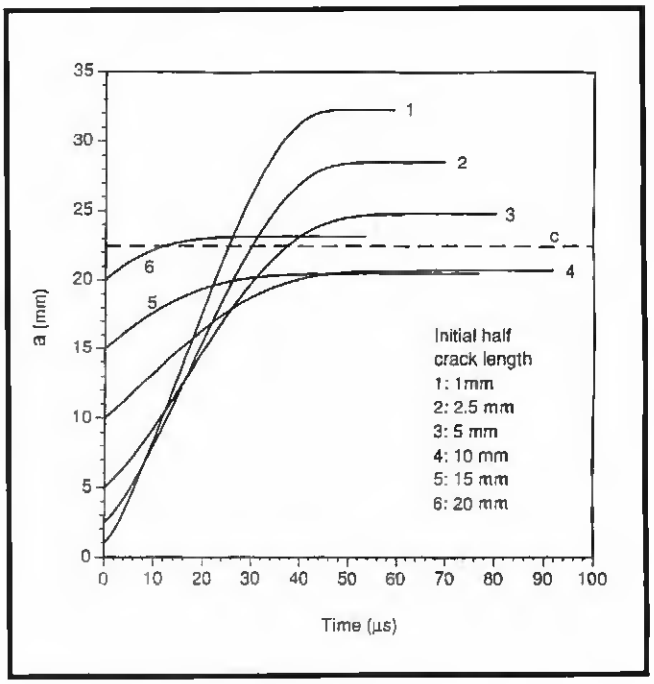

Fig. 11 — Instantaneous crack length as a function of time for sharp cracks with different initial crack lengths subjected to a nonuniformly distributed residual stress in a 4340 steel plate (dashed line shows c = 22.5 mm).

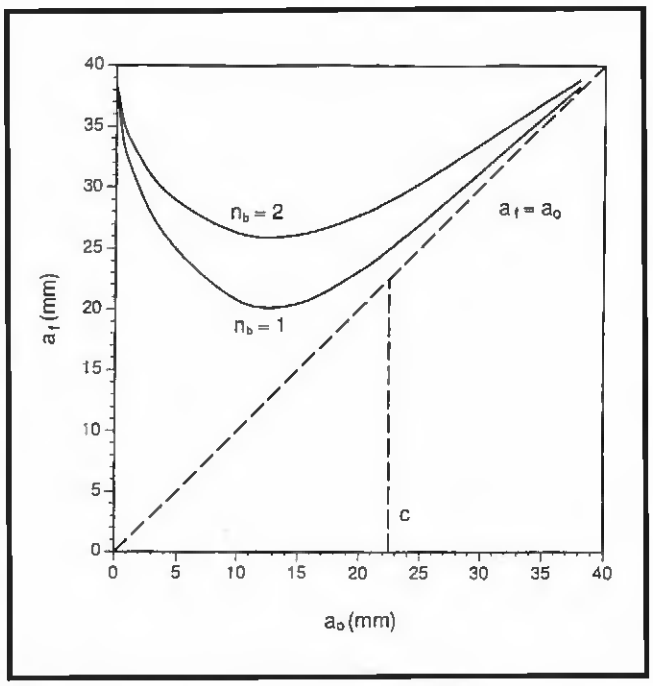

Fig. 12 — Relationship between final crack length and initial crack length.

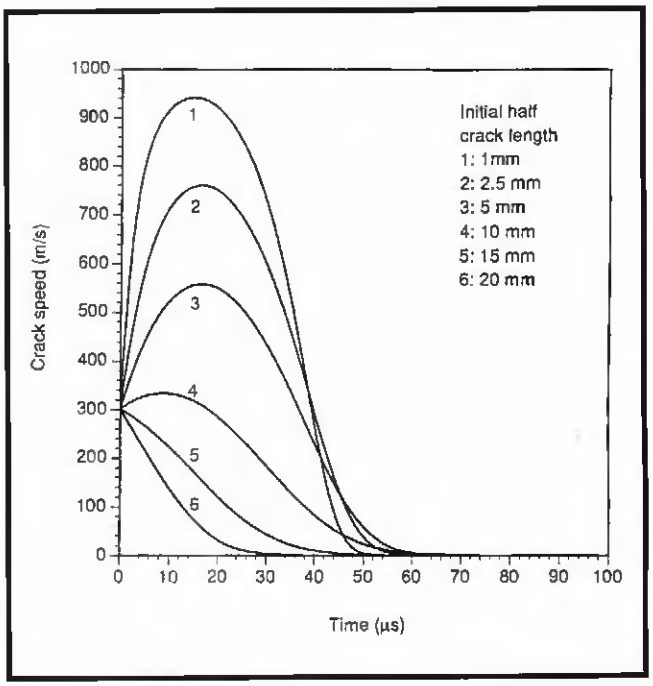

Fig. 13 — Crack speed behavior as a function of time for sharp cracks with different initial crack lengths subjected to a nonuniformly distributed residual stress in a 4340 steel plate (c = 22.5 mm).

after crack initiation, the crack speed for a long initial crack increases more slowly than that for a short one, and the crack speed decreases monotonically in Curves 5 and 6. Hence, the initial crack length has a significant effect on crack acceleration, while the bluntness parameter does not, as shown in Fig. 9.

Figure 14 illustrates the effect of initial crack length on the variation of dynamic stress intensity factor with time. Because these cracks are all sharp ($n_b = 1$), they have the same value of initiation fracture toughness with $K_{IO}' = K_{IO} = 61$ MPa $m^{1/2}$ and, as explained above, propagation starts in each case with the same initial speed v_o. It follows from Equations 13 and 3 that the initial value of $K_I(a_o,v_o)$ is independent of a_o. Comparing the peaks of the curves in Fig. 14, we note that the peak in Curve 1 is much higher than that in Curve 4, while there are no peaks for Curves 5 and 6. This is because of the high stress level required to extend a small initial crack. Finally, from the results in Figs. 11–14, we can conclude that a longer initial crack propagates more smoothly than a short one under the welding residual stress field.

In general, the crack starts to grow when the increasing residual stress, due to contraction after welding, reaches the critical value for crack initiation. Sometimes, even though the residual stress has been fully developed (*i.e.*, no more contraction in the weld occurs), the stress is still insufficient to drive the crack. However, after many hours or many days, delayed cracking may occur due to hydrogen degradation, which has the effect of reducing the fracture toughness, while the residual stress remains unchanged. This phenomenon is quite common in hydrogen-embrittlement-susceptible materials like AISI 4340 steel. In this case, we can still use Equation 17 to simulate crack propagation if the values of K_{IO} and K_{IM} for the degraded material are known.

As to the assumption of isotropy and homogeneity, we note that the phases in the heat-affected zone and the base metal in the weldment might be different, and thus the material properties and hence K_{IM}, K_{IO}, and wave speeds might vary with location and direction. Fortunately, the wave speeds are not very sensitive to microstructure or even to carbon content over a range of steels. However, the microstructure might have significant influences on K_{IM} and K_{IO}. To obtain more accurate results, the investigation of K_{IM} and K_{IO} as functions of microstructures is necessary in the future research.

This model is valid for a crack far from both ends of the weld. If that is not the case, the magnitude of residual stress will decrease due to redistribution of the stress when the crack extends. We could expect that the crack will stop sooner at a shorter final crack length, and that it is, thus, less critical in a weldment.

Conclusions

A fully dynamic approach has been used in the derivation of the crack-tip equation of motion in a weldment subjected to a nonuniform residual stress by employing the concepts of dynamic stress intensity factor and dynamic fracture toughness. The effects of crack speed, bluntness parameter, and the departure of arrest toughness from initiation toughness have been considered in the derivation.

A numerical analysis for a uniformly distributed stress was first performed. The results showed that both bluntness and the departure of K_{IM} from K_{IO} cause a jump in crack speed at the onset of crack growth, and the speed jump increases with the increase of these two effects. Numerical analysis also confirms that sharp cracks generally start from zero crack speed without a jump if there is no difference between K_{IM} and K_{IO}, followed by a sharp rise in the initial stages, and then level off to a constant crack speed.

The numerical simulation of the crack growth in the weldment under nonuniformly distributed welding residual stress has shown that there is a positive jump in crack speed and a negative jump in stress intensity factor at the onset of crack growth. Both dynamic stress intensity factor and crack speed subsequently increase, followed by decreases due to the reduction in the longitudinal residual stress. In general, a crack with a larger bluntness parameter or shorter initial crack length reaches a longer crack extension, a higher peak crack speed, and a higher dynamic stress intensity factor, while stopping in a shorter time. The initial crack speed and initial dynamic stress intensity factor increase with the increase of bluntness parameter, while they are independent of initial crack length.

The results can be used to provide information about crack propagation behavior as a source function in the study of acoustic emission due to crack growth.

References

1. Mott, N. F. 1948. Fracture of metals: theoretical consideration. *Engineering* 165: 16–18.

2. Berry, J. P. 1960. Some kinetic consideration of the Griffith criterion for fracture.

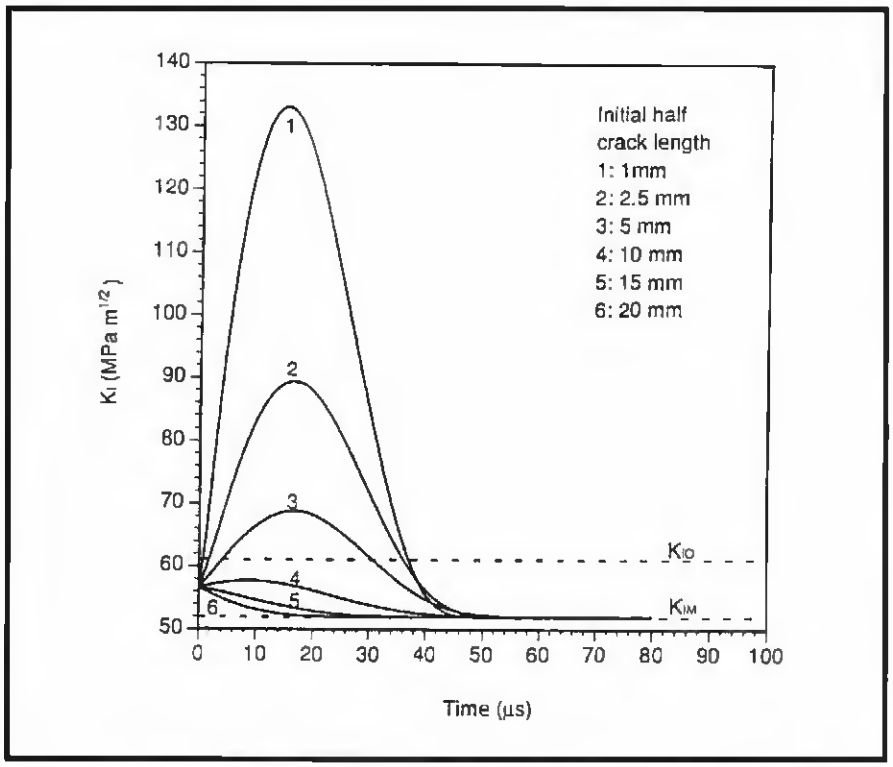

Fig. 14 — The variation of dynamic stress intensity factor as a function of time for sharp cracks with different initial crack lengths subjected to a nonuniformly distributed residual stress in a 4340 steel plate (c = 22.5 mm).

Journal of the Mechanics and Physics and Solids 8: 194–216.

3. Dulaney, E. N., and Brace, W. F. 1960. Velocity behavior of a growing crack. *Journal of Applied Physics* 31: 2233–2236.

4. Kanninen, M. F., and Popelar, C. H. 1985. *Advanced Fracture Mechanics*, Oxford University Press, New York.

5. Freund, L. B. 1972. Crack propagation in an elastic solid subjected to general loading — I. Constant rate of extension. *Journal of the Mechanics of Physics and Solids* 20: 129–140.

6. Freund, L. B. 1972. Crack propagation in an elastic solid subjected to general loading — II. Non-uniform rate of extension. *Journal of the Mechanics and Physics of Solids* 20: 141–152.

7. Roberts, D. K., and Wells, A. A. 1954. The velocity of brittle fracture. *Engineering* 178: 820–821.

8. Bergkvist, H. 1973. The motion of a brittle crack. *Journal of the Mechanics and Physics of Solids* 21: 229–239.

9. Rose, L. R. F. 1976. On the initial motion of a Griffith crack. *International Journal of Fracture* 12: 829–841.

10. Freund, L. B. 1990. *Dynamic Fracture Mechanics*, Cambridge, New York.

11. Xu, X.-P., and Needleman, A. 1993. Void nucleation by inclusion debonding in a crystal matrix. *Materials Science and Engineering* 1: 111–132.

12. Kostrov, B. V. 1975. On the crack propagation with variable velocity. *International Journal of Fracture* 11 (1): 47–56.

13. Dally, J. W. 1979. Dynamic photoelastic studies of fracture. *Experimental Mechanics* (10): 349–361.

14. Rosakis, A. J., Duffy, J., and Freund, L. B. 1984. The determination of dynamic fracture toughness of AISI 4340 steel by the shadow spot method. *Journal of the Mechanics and Physics of Solids* 32(4): 443–460.

15. Kobayashi, A. S., Ramulu, M., Dadkhah, M. S., Yang, K.-H., and Kang, B. S. J. 1986. Dynamic fracture toughness. *International Journal of Fracture* 30: 275–285.

16. Zehnder, A. T., and Rosakis, A. J. 1990. Dynamic fracture initiation and propagation in 4340 steel under impact loading. *International Journal of Fracture* 43: 271–285.

17. Josefson, B. L. 1985. Effects of transformation plasticity on welding residual stress fields in thin-walled pipes and thin plates. *Materials Science and Technology* 1(10): 904–908.

18. Masubuchi, K. 1960. Analytical investigation of residual stresses and distortions due to welding. *Welding Journal* 39(12): 525s to 537s.

19. Masubuchi, K., and Martin, D. C. 1966. Investigation of residual stresses by use of hydrogen cracking — Part II. *Welding Journal* 45(9):,401s to 418s.

20. Tatsukawa, I., and Oda, I. 1972. Distortions and residual stresses in arc welding. *Transactions of the Japan Welding Society* 3(2): 37–46.

21. Masubuchi, K. 1980. *Analysis of Welded Structures*, Pergamon Press, New York.

22. Barber, J. R. 1992. *Elasticity*, Kluwer, Dordrecht.

23. Tada, H., Paris, P. C., and Irwin, G. R. 1985. The stress intensity factor analysis of crack handbook, 2nd ed., Paris Productions, Inc. (and Del Research Corp.), St. Louis, Missouri.

24. Broek, D. 1986. *Elementary Engineering Fracture Mechanics*, 4th ed., Kluwer, Dordrecht.

25. Hahn, G. T., Hoagland, R. G., Rosenfield, A. R., and Sejnoha, R. 1974. Rapid crack propagation in a high strength steel. *Metallurgical Transactions* 5: 475–482.

26. Malkin, J., and Tetelman, A. S. 1971. Relation between K_{IC} and microscopic strength for low alloy steels. *Engineering Fracture Mechanics* 3: 151–167.

27. Datta, K. P. 1981. Sharp crack and blunt notch toughness behavior of quenched and tempered AISI 4340 steel. *Materials Science and Engineering* 51: 241–252.

28. Shukla, A., Agarwal, R. K., and Nigam, H. 1988. Dynamic fracture studies on 7075-T6 aluminum and 4340 steel using strain gages and photoelastic coatings. *Engineering Fracture Mechanics* 31(3): 501–515.